RZ 3964 (# ZUR1812-051) 12/29/2018
Physical Sciences 18 pages

Research Report

On the Early Stages of Soot Formation: Molecular Structure Elucidation by High-Resolution Atomic Force Microscopy

Mario Commodo[a], Katharina Kaiser[b], Gianluigi De Falco[c], Patrizia Minutolo[a], Fabian Schulz[b], Andrea D'Anna[c], Leo Gross[b]

[a]Istituto di Ricerche sulla Combustione, CNR, P.le Tecchio 80, 80125 Napoli, Italy

[b]IBM Research – Zurich, 8803 Rüschlikon, Switzerland

[c]Dipartimento di Ingegneria Chimica, dei Materiali e della Produzione Industriale, Università degli Studi di Napoli Federico II, P.le Tecchio 80, 80125 Napoli, Italy

DOI: 10.1016/j.combustflame.2019.03.042

Supplementary Materials for

ON THE EARLY STAGES OF SOOT FORMATION: MOLECULAR STRUCTURE ELUCIDATION BY HIGH-RESOLUTION ATOMIC FORCE MICROSCOPY

Mario Commodo[a, †], Katharina Kaiser[b, †], Gianluigi De Falco[c], Patrizia Minutolo[a], Fabian Schulz[b, *], Andrea D'Anna[c, *], Leo Gross[b]

[a] Istituto di Ricerche sulla Combustione, CNR, P.le Tecchio 80, 80125, Napoli, Italy

[b] IBM Research − Zurich, Säumerstrasse 4, 8803 Rüschlikon, Switzerland

[c] Dipartimento di Ingegneria Chimica, dei Materiali e della Produzione Industriale - Università degli Studi di Napoli Federico II, P.le Tecchio 80, 80125, Napoli, Italy

[†] These authors contributed equally.

*** Corresponding Authors**

F. Schulz (baf@zurich.ibm.com)

A. D'Anna (anddanna@unina.it)

S1. Burner and soot sampling system

A schematic view of the laminar premixed flame and of the sampling system is reported in Figs. S1a-c.

Soot particles suspended in the flame gases are extracted from the flame centerline by means of a horizontal tubular probe with a downward small orifice, i.e., 200 μm in diameter, where they rapidly mixed with a N_2 flow, thus being diluted 1:3000 (Fig. S1a). Downstream, particles were deposited on a quartz filter for off-line analysis (Fig. S1b) or sent to a sizing measurement system (Fig. S1c) consistent of an X-ray ion source to ionize the particles, a differential mobility analyzer to classify the particles based on their electrical mobility, and a faraday cup electrometer to count the size-selected particles. Gas temperature of the sampling line for off-line analysis was maintained at 80 °C and the sample collection lasted 14 hours to collect enough material on the filter for the analysis [1]. Soot particles were collected from the flame at 8 and 14 mm burner-to-probe separation distance (Z), which correspond to the particle nucleation and particle growth zone of the flame, respectively (see Fig. S1d). Images of the quartz filter after particle collection at Z = 8 mm and Z = 14 mm are reported in Figs. S1e and S1f. Clearly the quartz filter at Z = 8 mm appears brownish (Fig. S1e), whereas that at Z = 14 mm appears gray-to-black colored (Fig. S1f).

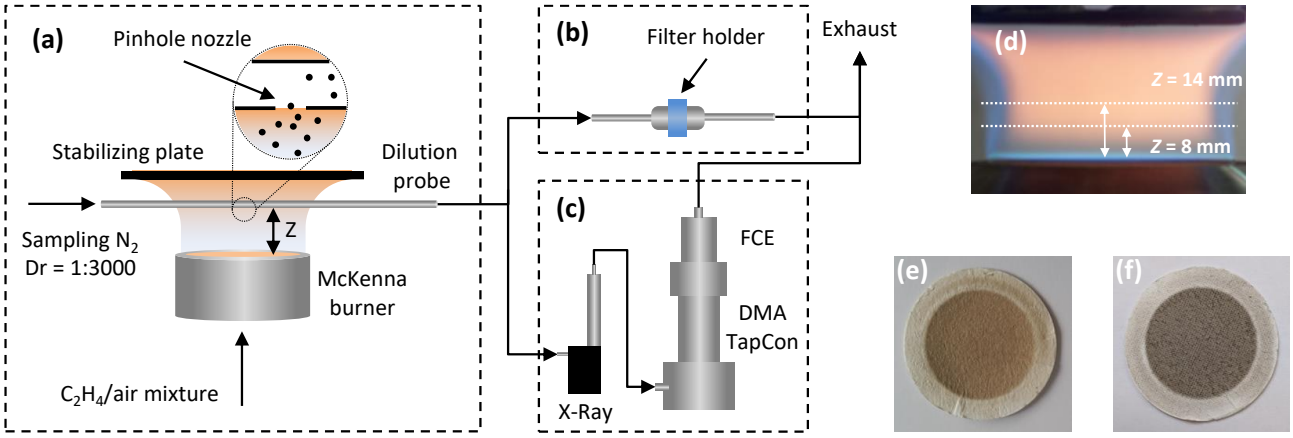

Figure S1. *(a) Diagrammatic sketch of the laminar premixed flame and the dilution probe sampling; (b) on-line particle collection on quartz filters; (c) differential mobility analysis set-up for particle size distribution measurements; (d) Image of the laminar premixed flame and the two probe-to-burner separation distances object of the current investigation; (e) Image of the quartz filter covered by incipient soot particles (Z = 8 mm); (f) Image of the quartz filter covered by primary soot particles (Z = 14 mm)*

S2. Flame temperature

Flame temperature was measured along the flame axis by an R-type thermocouple (Pt/Pt-13%Rh) with a spherical junction with a diameter of 300 μm. A rapid insertion procedure [2] and the

procedure described in detail in previous investigations [3,4] were adopted. Briefly, the time-resolved signal was recorded and the flame temperature was retrieved from the maximum recorded value, before the signal starts decreasing because of the coating of the thermocouple bead by soot. Temperature measurements were corrected for radiation heat losses following the procedure reported by Mc Enally et al. [5]. To account for the probe effect on the flame boundary conditions, a complete temperature profile along the flame has been measured for each positions of the probe in the flame.

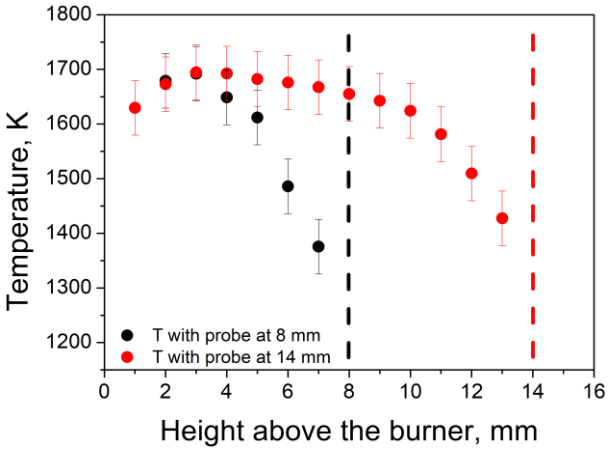

Figure S2. *Temperature profiles of the flame with probe positioned at the two probe-to-burner separation distances object of the current investigation.*

S3. Raman spectroscopy

Soot particles collected on the quartz filters (see Figs. S1e-f) have been preliminary analyzed by Raman spectroscopy by placing the filters, without any manipulation, under the microscope (Horiba XploRA) equipped with a 100X objective (NA0.9 Olympus), a Nd:YAG laser (λ = 532 nm, 12 mW maximum laser power at the sample) and a 200 µm pinhole for confocal photons collection. System calibration was performed against the Stokes Raman signal of pure silicon at 520 cm^{-1}. The power of the excitation laser beam was attenuated to 1% to avoid structural changes of the sample due to thermal decomposition when using an accumulation-exposure time of 5 cycles of 30 s each. A total of 10 spots were randomly selected over the filters to verify the homogeneity of the sample. Figure S3 reports the Raman spectra of the two soot samples, the red curves representing the average spectra.

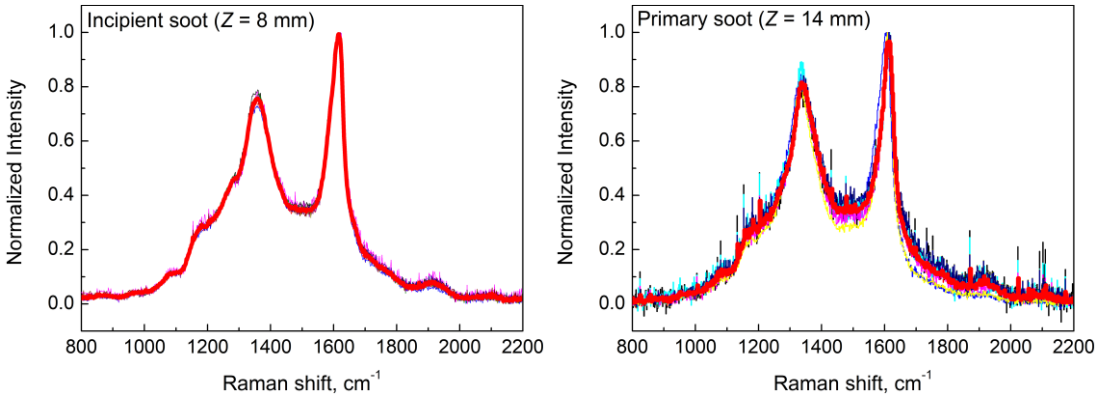

Figure S3. *Raman spectra of incipient (left panel) and primary (right panel) soot particles.*

In the case of highly disordered/amorphous carbon materials, i.e., for very small size of the graphite crystallites, and specifically for flame-formed soot particles [6,7], the following empirical expression correlates L_a, the average size of the aromatic units, with the relative intensity of the two Raman peaks, D and G, at about 1350 cm^{-1} and 1600 cm^{-1} respectively [8]:

$$L_a^2(\mathrm{nm}^2) = 5.4 \cdot 10^{-2} \cdot E_L^4(\mathrm{eV}^4) \frac{I(\mathrm{D})}{I(\mathrm{G})} \qquad \text{(S1)}$$

where E_L is the energy of the incident photon. From the measured Raman spectra, we obtain a I(D)/I(G) value of 0.76 ± 0.02 for the incipient soot, which results in L_a = 1.10 nm using Eq. (1), and I(D)/I(G) = 0.84 ± 0.02 for primary soot, which results in L_a = 1.16 nm. The value of L_a for soot molecules does not increase significantly between incipient and primary soot particles. Furthermore, it roughly corresponds to the size of ovalene, and reasonably well agrees with the average size of the aromatic building blocks imaged by AFM.

S4. Structure assignment

Assigned structures for the full set of the identified molecular constituents of soot particles are reported in Fig. S4.1 for particles collected at Z = 8 mm and Fig. S4.2 for particles collected at Z = 14 mm. The structure assignment, especially for the different moieties, is based on experimental data on model compounds from previous studies as well as measurements presented in this work. Examples of unidentified entities are reported in Fig. S4.3.

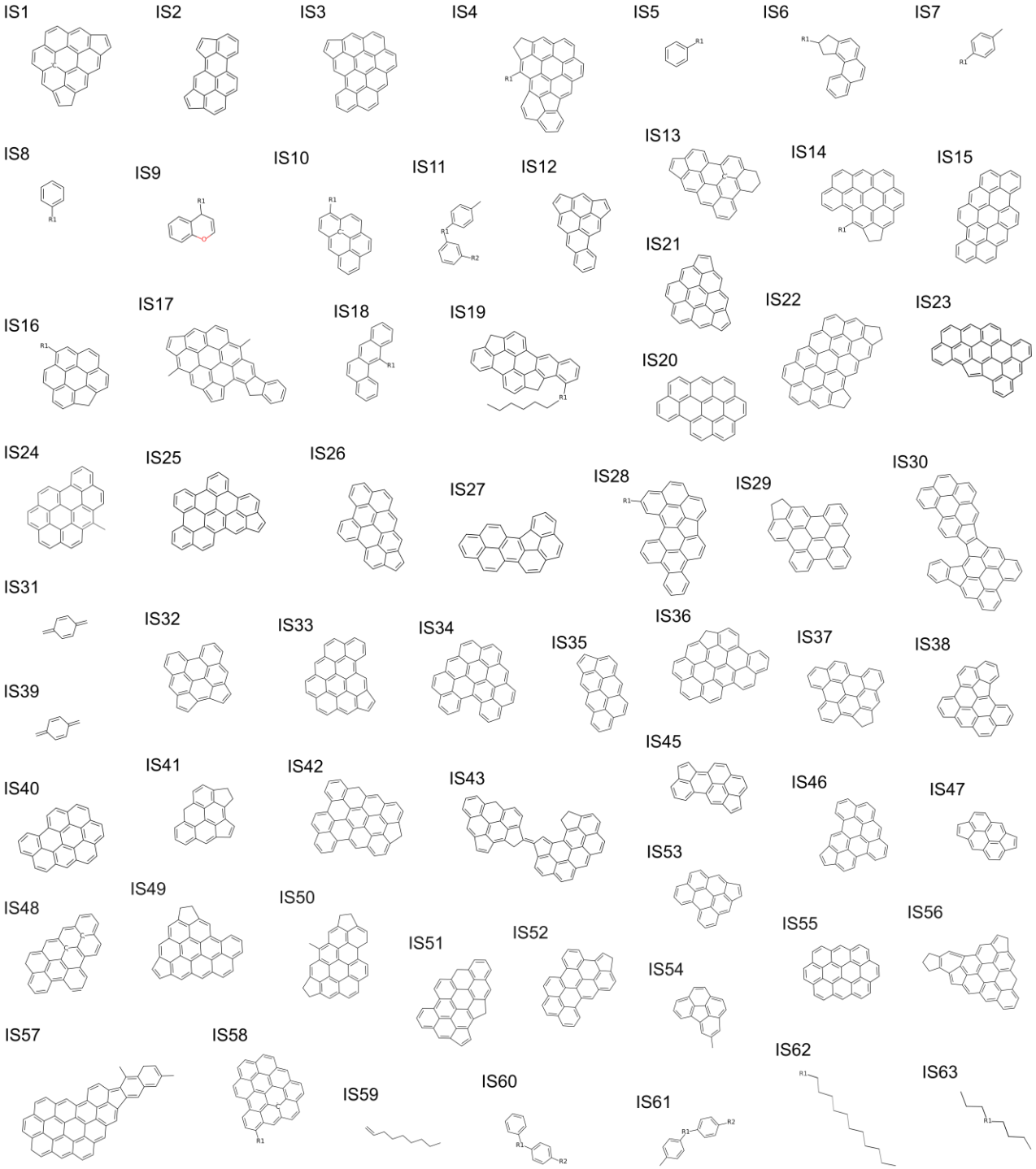

Figure S4.1. *Assigned structures for the PAHs and chains found in incipient soot molecules (Z = 8 mm burner-to-probe separation distance) shown in Fig. 2.*

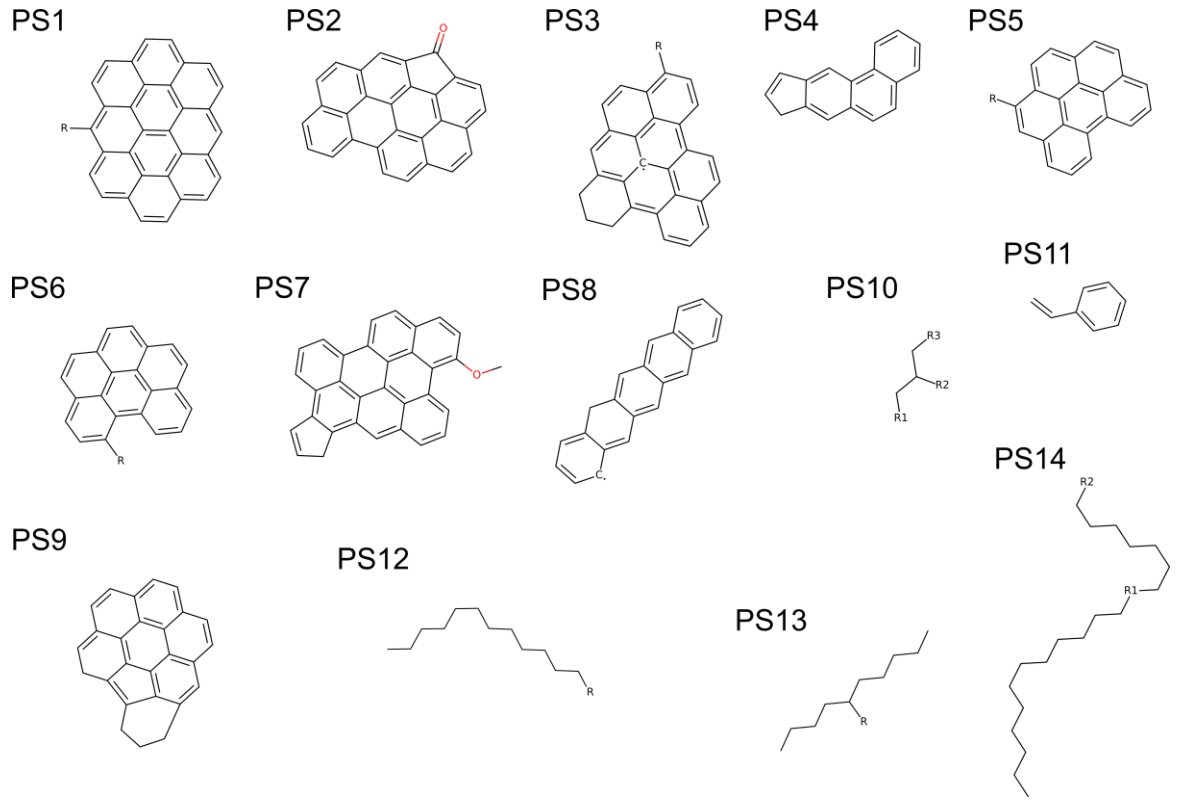

Figure S4.2. *Assigned structures for the PAHs and chains found in primary soot molecules (Z = 14 mm burner-to-probe separation distance) shown in Fig. 3.*

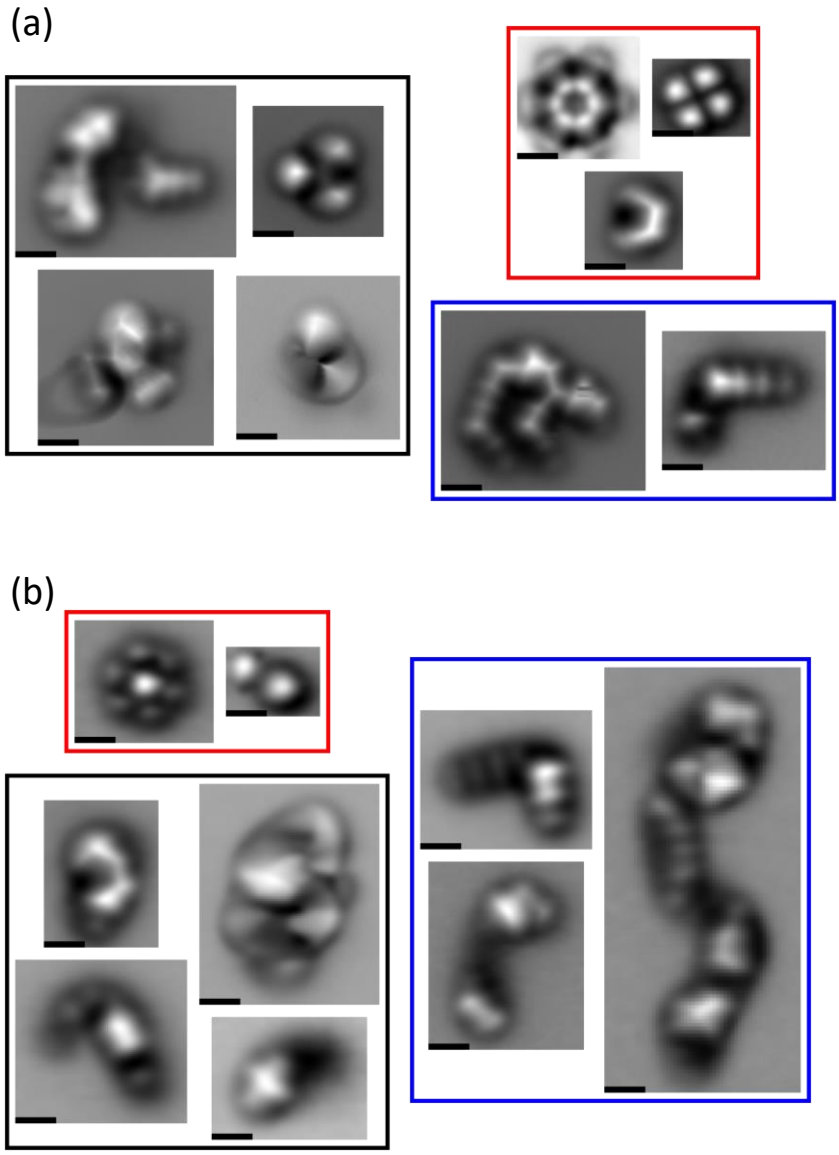

Figure S4.3. *Examples for AFM images of unidentified chains (blue), 3D structures (black), and too small/mobile molecules (red). (a) Molecules from incipient soot particles (Z = 8 mm); (b) Molecules from primary soot particles (Z = 14 mm). All scale bars are 0.5 nm.*

References

(1) F. Schulz, M. Commodo, K. Kaiser, G. De Falco, P. Minutolo, G. Meyer, A. D'Anna, L. Gross. *Proc. Combust. Inst.* 37 (2019) 885-892.
(2) J.H. Kent, H.Gg. Wagner, *Combust. Sci. Technol*. 41 (1984) 245–269.
(3) A.D. Abid, N. Heinz, E.D. Tolmachoff, D.J. Phares, C.S. Campbell, H. Wang, *Combust. Flame* 154 (2008) 775–788.
(4) G. De Falco, M. Commodo, A. D'Anna, P. Minutolo, *Proc. Combust. Inst.* 36 (2017) 763-770.
(5) C.S. McEnally, U.O. Koylu, L.D. Pfefferle, D.E. Rosner, *Combust. Flame* 109 (1997) 701–720.
(6) P. Minutolo, M. Commodo, A. Santamaria, G. De Falco, A. D'Anna, *Carbon* 68 (2014) 138–148.
(7) M. Commodo, P.H. Joo, G. De Falco, P. Minutolo, A. D'Anna, Ö. L. Gülder, *Energy Fuels* 31 (2017) 10158−10164.
(8) A.C. Ferrari, J. Robertson, *Phil. Trans. R. Soc. Lond.* A (2004) 362, 2477–2512.

Combustion and Flame 205 (2019) 154–164

Contents lists available at ScienceDirect

Combustion and Flame

journal homepage: www.elsevier.com/locate/combustflame

On the early stages of soot formation: Molecular structure elucidation by high-resolution atomic force microscopy

Mario Commodo[a,1], Katharina Kaiser[b,1], Gianluigi De Falco[c], Patrizia Minutolo[a], Fabian Schulz[b,*], Andrea D'Anna[c,*], Leo Gross[b]

[a] Istituto di Ricerche sulla Combustione, CNR, P.le Tecchio 80, 80125 Napoli, Italy
[b] IBM Research – Zurich, Säumerstrasse 4, 8803 Rüschlikon, Switzerland
[c] Dipartimento di Ingegneria Chimica, dei Materiali e della Produzione Industriale, Università degli Studi di Napoli Federico II, P.le Tecchio 80, 80125 Napoli, Italy

ARTICLE INFO

Article history:
Received 4 January 2019
Revised 1 March 2019
Accepted 28 March 2019
Available online 13 April 2019

Keywords:
PAH, Soot
Ultrafine particles
Nucleation
Atomic force microscopy
Atomic resolution

ABSTRACT

The early stages of soot formation, namely inception and growth, are highly debated and central to many ongoing studies in combustion research. Here, we provide new insights into these processes from studying different soot samples by atomic force microscopy (AFM). Soot has been extracted from a slightly sooting, premixed ethylene/air flame both at the onset of the nucleation process, where the particle size is of the order of 2–4 nm, and at the initial stage of particle growth, where slightly larger particles are present. Subsequently, the molecular constituents from both stages of soot formation were investigated using high-resolution AFM with CO-functionalized tips. In addition, we studied a model compound to confirm the atomic contrast and AFM-based unambiguous identification of aliphatic pentagonal rings, which were frequently observed on the periphery of the aromatic soot molecules. We show that the removal of hydrogen from such moieties could be a pathway to resonantly stabilized π-radicals, which were detected in both investigated stages of the soot formation process. Such π-radicals could be highly important in particle nucleation, as they provide a rational explanation for the binding forces among aromatic molecules.

1. Introduction

Despite the increasing contribution of renewable energy sources, fossil fuel combustion remains the primary player for the worldwide energy production [1]. Examples include the power generation using fossil fuels like natural gas or oil, the use of combustion in the automotive sector as well as for home heating and cook-stoves appliances and the use of gas-turbine combustors for aero-transportation.

Combustion generates heat by means of exothermic reactions which in turn, ideally, lead only to the formation of carbon dioxide and water. However, in real combustion devices the presence of local fuel-rich conditions promotes the formation of harmful carbonaceous by-products, in particular carbon nanoparticles, namely soot.

Soot particles have been investigated over the last decades by the scientific community for their detrimental health effects and for affecting the Earth radiation balance. Numerous studies have clearly indicated that combustion-formed particulates are responsible for several adverse health effects [2–4]. Among those, particles with sizes in the order of a few nanometers, typically referred to as ultrafine particles, are known to be particularly dangerous [5]. Furthermore, soot particles can severely affect the climate [6]. Their emission into the atmosphere influences light absorption and cloud formation as well as the albedo and melting properties of snow and ice covers [6,7]. For these reasons, a deeper understanding of the chemical constituents as well as the processes responsible for the formation of such particles would be highly beneficial.

The formation and evolution of soot particles in fuel-rich flames are the result of a complex mechanism including both chemical and physical processes. These are: initial gas-phase reactions, gas to condensed-phase transition corresponding to particle nucleation, particle mass and size growth through coagulation/coalescence, heterogeneous surface reactions and condensa-

* Corresponding authors.
E-mail addresses: baf@zurich.ibm.com (F. Schulz), anddanna@unina.it (A. D'Anna).
[1] Both the authors contributed equally to this work.

https://doi.org/10.1016/j.combustflame.2019.03.042

tion of gaseous species and finally, carbonization/dehydrogenation reactions. When oxygen is available in the flame, particle oxidation occurs parallel to the above reported mechanisms. The whole mechanism takes place at high temperature and on a time scale of the order of a few milliseconds. Therefore, understanding the soot formation process in fuel-rich combustion is a great challenge.

The process starts with the decomposition reactions of the fuel molecules, i.e., pyrolysis and oxidation, and subsequent recombination and cyclization reactions lead to the formation of polycyclic aromatic hydrocarbons (PAHs). It is generally understood that the growth of PAHs in flames occurs by repetitive hydrogen abstraction followed by acetylene (C_2H_2) addition [8], known as the hydrogen abstraction acetylene addition (HACA) mechanism [9,10]. These aromatic molecules can exhibit many different configurations, i.e., different sizes, shapes and functionalities. Through chemical and/or physical clustering, they act as precursors of incipient soot particles [10–12]. Over the years, great efforts have been made to understand the fundamentals of the early steps of soot formation and some mechanisms have been proposed to explain the gas-to-particle transition [10–12]. Two well-established mechanisms involve either the chemical reactions of two or more PAHs and their radicals to form polymer-like cross-linked structures, or physical clusters of two or more PAHs bound through van der Waals forces. Both pathways may coexist with a relative relevance depending on the combustion conditions/environments such as temperature and gas-phase chemical composition [10–12]. Recently, a radical chain propagation mechanism involving resonantly stabilized radicals (RSRs) has been proposed for molecular mass growth and clustering with the formation of covalently bound complexes [13]. Moreover, a mechanism involving aromatic π-radicals with localized π-electrons in the nucleation and growth process of soot was also suggested by Wang [12].

Just-nucleated soot particles have typical sizes of a few nanometers [14–16]. They are mainly formed just downstream of the flame front in aliphatic fuel flames, although they can persistently nucleate in the post-flame region [17,18]. After nucleation, particles undergo further growth, reaching sizes of the order of 10 – 20 nm, followed by coagulation/agglomeration and formation of chain-like aggregates. During this process, the chemical/structural composition of the soot particles can further change, as is often observed in terms of different hydrogen to carbon ratio, nanoscopic structure and optical properties [19–21].

To simplify this highly complex problem and to allow controlling operative parameters with high precision, the majority of the studies aimed at investigating the soot formation mechanism are performed in laboratory premixed or diffusion flames of gaseous hydrocarbons. In a laminar premixed flame, the different stages of the soot formation process can be followed at increasing distances to the burner. Hence, collecting particles at different burner-to-probe separation distances provides snapshots of the particles involved in this intricate process.

In a recent work [22], we analyzed soot particles extracted from the nucleation zone of a premixed flame using high-resolution atomic force microscopy (AFM) and scanning tunneling microscopy/spectroscopy (STM/STS). AFM is susceptible to forces and can thus be used to probe the short-range repulsive forces above molecules that emanate from overlapping wavefunctions (Pauli repulsion), yielding high contrast on covalent bonds and atoms. For tip passivation, carbon monoxide (CO) is widely used [23]. Considering that bending of the CO might lead to distortions [24], it additionally enhances the contrast due to its flexibility. This method can be applied to identify the atomic structure of natural compounds and complex molecular mixtures [25–27], discriminate the bond order within single molecules [28], or follow the intermediate steps of on-surface reactions [29,30]. STM, however, is sensitive to the local density of states, providing access to molecular orbital densities [31–33].

Using these techniques, we were able to detect and analyze PAH molecules and their radicals present in incipient soot particles. While in the previous work [22] we showed selected, characteristic structures, here we provide an in-depth discussion of all observed structures as well as a comparison to a model compound, confirming our results on saturated peripheral penta-rings. Additionally, another characteristic stage of the soot formation process, namely particle growth, has been investigated by collecting particles from the flame at different burner-to-probe distances, thus gaining further insight into the soot formation mechanism.

Our results conduce to the understanding of soot formation by providing a framework of molecules that are decisively contributing to this process, and thereby deepen the knowledge of its underlying chemistry at the molecular level. In the long run, this information could eventually help to improve technologies relying on fuel combustion to prevent the emergence of harmful by-products.

2. Experimental system

Soot nanoparticles were generated in a laminar premixed flame burning an ethylene-air mixture. In this flame reactor, the temperature and the species concentrations only depend on the height above the burner, which directly relates to the flame residence time. The cold gas velocity was set at 9.8 cm/s and carbon to oxygen (C/O) atomic ratio was fixed at 0.67, i.e., equivalence ratio $\Phi = 2.03$.

Soot particles suspended in burned combustion gases were extracted from the flame centerline using a high-dilution horizontal tubular probe [14]. Flame temperature profiles measured with and without probe are reported in the supplementary materials (Fig. S2). The combustion products were sampled through a very small orifice, i.e., 200 µm in diameter, located on the bottom side of the probe, and rapidly mixed with N_2, thus providing a dilution ratio (DR) of 1:3000 [14]. This sampling procedure prevents particles from coagulating and allows the quenching of chemical reactions throughout the sampling line [17]. Soot particles were collected from the flame at 8 and 14 mm burner-to-probe separation distance (Z), which correspond to the particle nucleation and particle growth zone of the flame, respectively. In the following, we will therefore refer to molecules detected in the particles extracted from the nucleation zone ($Z = 8$ mm) as incipient soot molecules (IS), and to molecules from particles collected in the growth zone ($Z = 14$ mm) as primary soot molecules (PS).

The particle size distributions (PSDs) were measured on-line using a differential mobility analyzer (DMA) system composed by an aerosol classifier Vienna-type DMA (TapCon 3/150) that allows particle classification within the size range of 1–40 nm, an X-ray diffusion charging source (TSI Aerosol Neutralizer 3088), and a Faraday cup electrometer for particle counting. For the off-line analyses, a stainless steel aerosol filter holder (Merk–Millipore Mod. XX5004700) containing a quartz filter (Whatman QMA–grade, 47 mm) was positioned on-line downstream of the dilution tubular probe for soot collection. Gas temperature at the filter location was 80 °C. The sample collection lasted 14 h in order to collect enough material on the filter for the off-line analysis [22]. A schematic view of the burner and soot sampling is reported in the supplementary materials (Fig. S1). Soot particles collected on the quartz filters were preliminarily analyzed by Raman spectroscopy (results are reported in the supplementary materials, Fig. S3).

The STM and AFM measurements were carried out in a home-built combined STM/AFM setup operating under ultra-high vacuum (UHV) conditions ($p \approx 1 \times 10^{-10}$ mbar) and at low temperatures ($T \approx 5$ K). The microscope was equipped with a qPlus quartz

cantilever [34] operated in the frequency modulation mode [35]. The microscope tip consisted of a PtIr-wire (25 µm in diameter), which was sharpened using a focused ion beam followed by *in situ* indentations into the bare Cu surface to prepare a clean and atomically sharp tip.

All STM images were acquired in constant-current mode with the bias voltage V applied to the sample, while AFM images were taken in constant-height mode at $V = 0$ V. For AFM imaging, the tip apex was passivated by picking up a single CO molecule from the surface [36]. As a substrate, we used a Cu(111) single crystal partially covered with (100)-oriented, two monolayer (ML) thick NaCl islands, denoted as NaCl(2ML)/Cu(111). An exemplary STM overview image has been reported elsewhere [22].

The soot particles were deposited on the substrate via sublimation from a piece of Si-wafer. To this end, the particles were applied on the wafer by gently pressing the quartz filter containing the collected material onto the wafer. The wafer was subsequently transferred into the UHV system and positioned in front of the cold sample ($T \approx 7$ K). For sublimation of the molecules, the wafer was flash-annealed via resistive heating from room temperature to approximately 900 K within a few seconds. This rapid heating can promote the process of evaporation over the decomposition [37,38] and has been shown to work reliably for molecules with masses up to about 600 Da [39,40].

3. Results

In the early zones of the post-flame region, i.e., $Z = 8$ mm, the PSD in number concentration is characterized by a mono-modal distribution, with sizes mostly below 4 nm and maximum number density between 2 and 3 nm, as shown in Fig. 1. This mode comprises the first detectable particles and it is usually referred to as incipient soot [14–16]. At increasing Z, the PSD starts exhibiting a bimodal shape, with a first mode similar to the one observed at $Z = 8$ mm, and a second one, whose modal value increases with Z and reaches 12 nm at $Z = 14$ mm. This second mode is therefore believed to constitute the primary soot particles. It is important to keep in mind that, considering the cubic dependence of the particle mass/volume on particle diameter, the mass of carbon materials collected at these flame locations mainly consists of primary soot particles, although PSDs at heights larger than 8 mm are clearly bimodal with a large number of incipient soot particles.

Figure 2 reports the full set of the identified molecular constituents of incipient soot particles collected at $Z = 8$ mm and measured by AFM. The proposed structures are reported in the supplementary materials (Fig. S4.1). About 120 molecules were analyzed by AFM; 44% of which were univocally determined PAHs and 11% were substituted benzenes and chain-like structures with substantial aliphatic character. The unidentified structures (see supplementary materials, Fig. S4.3 for example molecules) consisted of molecules which were too mobile and/or too small (about 26%) to be identified and 3D structures (about 19%) with sizes roughly comparable to the identified PAHs.

The images in Fig. 2 reveal that the molecular constituents of the incipient soot present the following features (see also Schulz et al. [22]):

- The molecular masses range from 200 to 700 Da (14–60 C-atoms) with a large number of molecules with masses around 300–400 Da (24–30 C-atoms).
- A large fraction of the molecules contains fused six-ring units organized in almost entirely *peri*-condensed structures with zigzag and free edges. Many molecules exhibit one or two arm-chair edges while only very few bay-edges and no fjord-edges are observed.

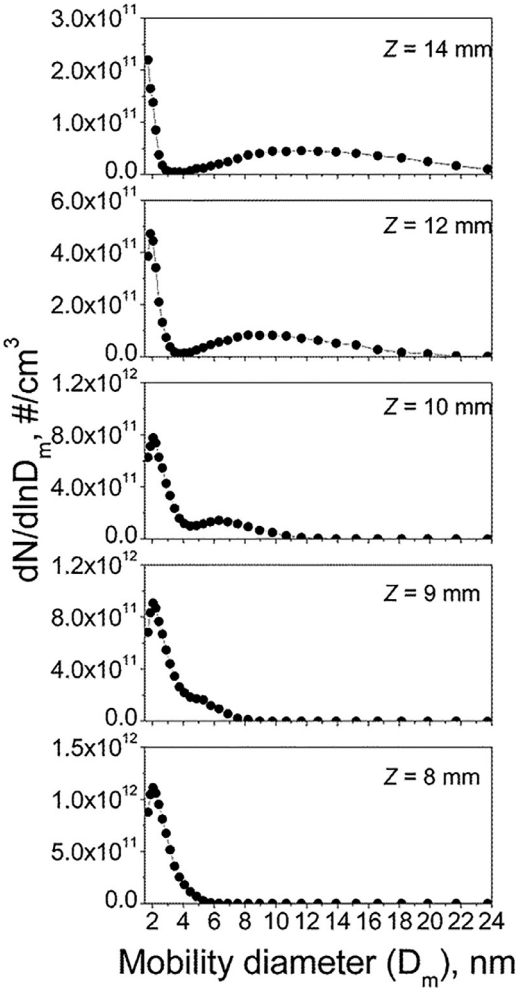

Fig. 1. Particle size distributions at different burner-to-probe separation distances. Note that PSDs were corrected for dilution and particle diffusion losses in the probe following the procedure reported in [14].

- Several molecules exhibit aliphatic branches – mostly methyl (-CH_3) groups.
- Most of the imaged molecules contain penta-rings on their periphery while a smaller fraction shows penta-rings (partially) embedded into the aromatic structure.
- A large presence of sp^3 hybridized carbons forming C–H bonds in methylene-type groups is observed in peripheral penta-rings, and in some cases also in peripheral six-rings.

The analysis and identification of the molecules constituting the particles after coagulation/growth (primary soot at $Z = 14$ mm) turned out to be more challenging. For these particles, sublimation appeared to be a major bottleneck, although Raman spectroscopy measurements predicted an average size for their aromatic constituents similar to that of incipient soot ($Z = 8$ mm) (see supplementary materials S3 for more details about the Raman spectroscopy measurements). The analyzed sample mostly contained very bulky or small/mobile molecules and aliphatic chains, which we attribute to fragmentation of the molecules during the sublimation process. Only few aromatic molecules (about 7%) could be identified; the corresponding AFM images are shown in Fig. 3. Although the resolved aromatics are of limited statistical significance due to their small number, the average size of the molecules that could be analyzed by AFM is similar to that of the molecules from incipient soot. Besides, aliphatic groups and a few penta-rings were also detected. Different from the molecules found

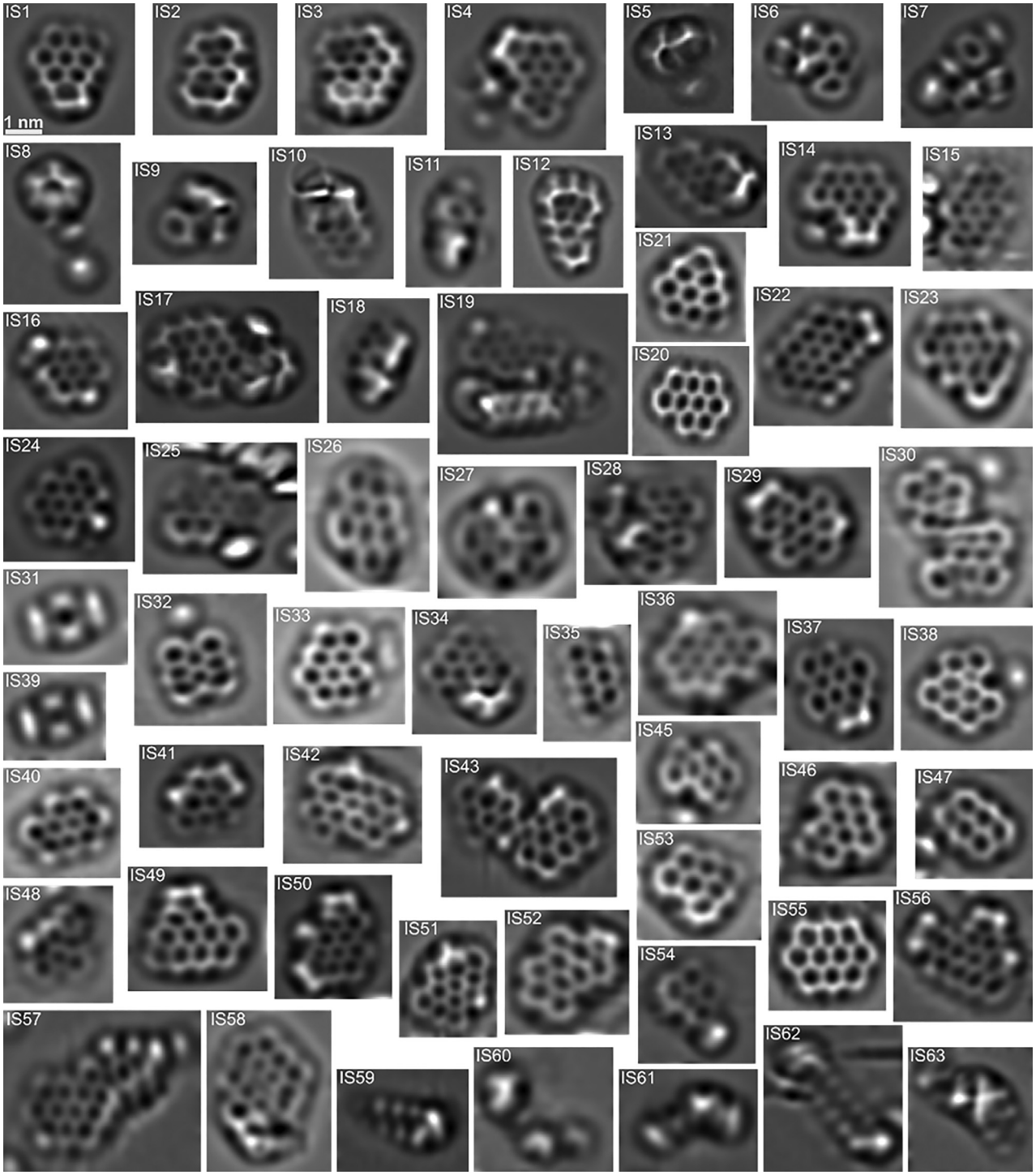

Fig. 2. Laplacian-filtered constant-height CO-tip AFM images of all identified molecules found in soot particles collected at $Z = 8$ mm (incipient soot particles). The following molecules were shown in ref. [22]: **IS1** (**M4**), **IS2** (**M5**), **IS8** (**M7**), **IS19** (**M6**), **IS22** (**M3**), **IS24** (**M2**), **IS43** (**M10**), **IS53** (**M1**), **IS59** (**M9**), **IS60** (**M8**). The label in the brackets corresponds to the respective labeling used in ref. [22]. All images have the same scale.

in incipient soot, a few of the imaged molecules (**PS2, PS7**) contain oxygen atoms (see supplementary materials Fig. S4.2 for structure assignment).

4. Discussion

4.1. Soot molecules: size and moieties

Our results, obtained by AFM/STM, show a large complexity of the molecular constituents of soot collected in a laminar premixed flame, ranging from small aliphatic chains/substituted benzene molecules to few very large polyaromatic compounds containing up to 52 carbon atoms (**IS30** and **IS43** in Fig. 2).

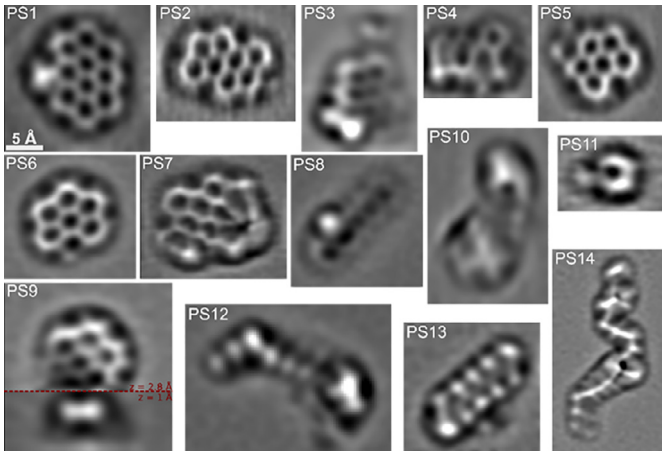

Fig. 3. Laplacian-filtered AFM images of identified PAH molecules and aliphatic chains/substituted benzenes found in the soot particles collected at $Z = 14$ mm (primary soot particles). The red dashed line in **PS9** indicates a change in tip-sample distance by 1.8 Å. All images have the same scale. (For interpretation of the references to color in this figure legend, the reader is referred to the web version of this article.)

These results are in good agreement with previous investigations by mass spectrometry and spectroscopic and/or microscopic techniques. Compositional analysis of soot by mass spectrometry was reported by Dobbins and co-workers in a series of seminal works in the late nineties [41,42]. They identified PAHs containing 16–32 carbon atoms (202–472 Da molecular mass range) as the molecular constituents of soot particles from a laminar diffusion flame. The analyzed molecules agreed well with those predicted by Stein and Fahr [43] as the most thermodynamically stable PAHs at flame temperatures, i.e., the stabilomers. However, a series of aerosol mass spectrometry (AMS) studies coupled with tunable synchrotron vacuum-ultraviolet (VUV) radiation, recently pointed out the insufficiency of the stabilomer grid in describing the actual complexity of the molecular structures participating in the soot formation mechanism [44–47]. Similar ranges of molecular masses were also observed on soot surfaces by Bouvier et al. [48] using laser desorption/laser ionization/TOF-MS and by Öktem et al. [49] probing soot molecular chemistry in laminar premixed flames by photoionization aerosol mass spectrometry (PIAMS). Analogous results were also obtained by spectroscopic diagnostics and microscopy. Studies based on ultraviolet-visible light absorption spectroscopy followed by optical band-gap analysis [14,50,51], Raman spectroscopy [14,52] and HR-TEM [50,52] analysis of flame soot indicated that the aromatic domains forming the particles are of the order of 1 nm in size. This corresponds roughly to the size of ovalene ($C_{32}H_{14}$) and is thus in very good agreement with the average molecular mass of the molecules imaged by AFM/STM, shown in Figs. 2 and 3.

A second relevant observation retrieved form our AFM/STM analysis is the presence of molecules with aliphatic branches, mostly in the form of methyl groups. This is the case for the molecules: **IS5, IS6, IS4, IS10, IS14, IS16, IS17, IS18, IS19, IS24, IS28, IS50, IS54, IS57, IS58** (see Fig. 2) for incipient soot and **PS1, PS3, PS5, PS6** for primary soot particles (see Fig. 3 and the supplementary materials Fig. S4.1 and Fig. S4.2 for the structure assignment). The presence of an appreciable contribution of aliphatic components in the aromatic molecules constituting soot was already proposed by various authors using different techniques. Öktem et al. [49] observed that the intensities of aliphatic components and PAHs were of the same order of magnitude at low heights in the flame; however, the aliphatic components become much more abundant at the end of the flame where the PAH signal was hardly detected. This also matches our observations especially in primary soot particles, where only 7% of the molecules investigated by STM/AFM are PAHs but a significantly larger fraction are aliphatics. Using thermal desorption-chemical ionization time-of-flight mass spectrometry, the nature of the aliphatic constituents in soot was later suggested to be in the form of alkylated aromatics with molecular weights spanning from 200 to 900 Da [53]. The presence of aliphatic moieties and their relevance in the soot growing mechanisms was also evidenced by infrared spectroscopy analysis [54,55], nuclear magnetic resonance spectroscopy (NMR) [56], and X-ray photoemission spectroscopy [21] of flame-formed soot particles. Aliphatic CH vibrations were also measured by surface-enhanced Raman spectroscopy in grown soot particles [57]. Our AFM/STM results represent, however, the first direct observation of a rather large fraction of soot constituents in the form of alkylated aromatics. Such alkyl functionalities are mainly in the form of methyl groups, although larger chains have also been observed. The importance of substituted aliphatic chains in the physical agglomeration of PAHs leading to soot formation has also been theorized by Elvati and Violi [58], performing molecular dynamics simulations.

4.2. Five-membered rings

The third relevant observation obtained from the soot molecules reported in Figs. 2 and 3 is the presence of an appreciable number of aromatic molecules incorporating pentagonal rings.

The role of five-member rings in the growth of carbon structures in combustion has long been explored [59,60]. Johansson et al. [47] theorized that the most abundant PAH structures at 202 Da and 226 Da contain five-membered rings instead of only six-membered rings. The inclusion of five-membered rings was already hypothesized by Öktem et al. [49]. It was noticed that "*all the isomers at 250 m/z contain five-membered rings, with two structures containing two each*". The 250 *m/z* peak may comprise, for example, molecules like **IS47** (Fig. 2). The location of pentagonal rings within the aromatic units has been shown to have a remarkable effect on the electronic structure of the molecule itself [61,62]. Motivated by the prediction that curved PAHs may have a dipole moment, Kraft and coauthors [62] investigated the impact of PAH curvature induced by the inclusion of five-membered rings on the process of soot particle formation.

Over the entire set of analyzed incipient soot molecules, we observed some partially internal pentagonal rings, such as in **IS54**, resembling methyl-benzo[*ghi*]fluoranthene, and some other similar larger structures (**IS4, IS27, IS28, IS38**), as illustrated in Fig. 4(a). The aromatic molecules extracted from soot at the nucleation point do not present a significant curvature. This finding is consistent with the results of Raman spectroscopy on similar soot samples reported in a previous work [21], showing that rather flat aromatic islands are present at the nucleation stage, while the graphitic lamellae become more distorted/curved in grown particles formed later in the flame. The observation that aromatics stay flat for a while and start developing curvature later in the flame is also consistent with the theoretical/modeling predictions of Whiteside and Frenklach [60]. Therefore, it is likely that, starting from structures such as **IS4, IS27, IS28, IS38, IS54,** some degree of curvature may occur at higher residence time, i.e., higher *Z*, due to further molecular growth. For instance, **IS54** could significantly curve by the addition of one acetylene (C_2H_2) molecule and subsequent ring closure, forming corannulene ($C_{20}H_{10}$). An additional type of partially embedded pentagonal rings, in the form of fluoranthene-type benzenoid systems, was also detected, see molecules **IS30** and **IS57** (Fig. 4(b)).

Different types of peripheral pentagonal rings are observed, as sketched in Fig. 5(a)–(d). Figure 5(a) shows aromatics with pen-

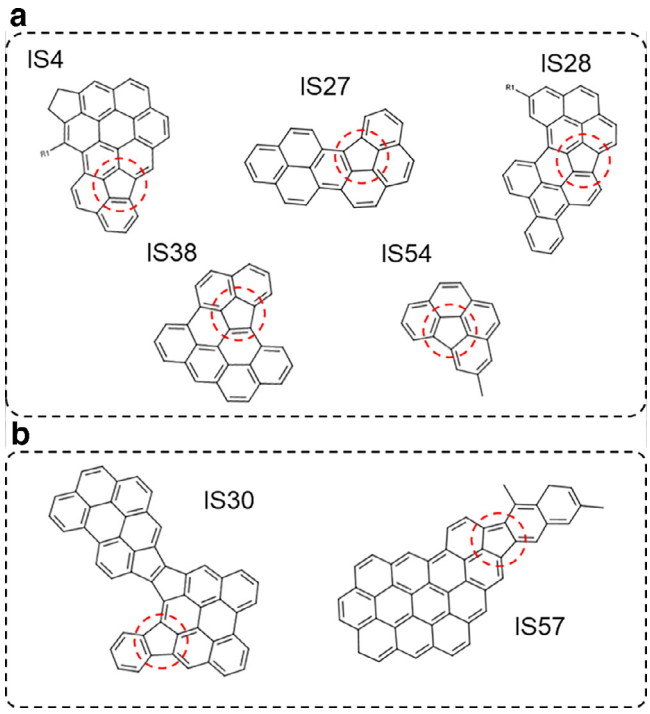

Fig. 4. Chemical structures of molecules with partially internal penta-rings assigned on the basis of the AFM measurements shown in Fig. 2: (a) molecules incorporating benzo[*ghi*]fluoranthene-type moieties; (b) molecules incorporating fluoranthene-type moieties.

tagonal rings in acenaphthylene-type configuration. They can be formed by hydrogen abstraction followed by acetylene (C_2H_2) addition on a zigzag edge of an aromatic structure [8,60,63]. In this case, the C–H bond is of vinylic-type, i.e., carbon is sp^2 hybridized. Interestingly, several imaged molecules presented evidence of pentagonal rings with methylene-type C–H bonds, i.e., carbon is sp^3 hybridized (Fig. 5(b)–(d)). Those are likely to be formed by hydrogen abstraction followed either by ethylene (C_2H_4) or vinyl (C_2H_3) addition on a zigzag edge [64] to form the acenaphthene-type configuration (Fig. 5(b)), or by methyl (CH_3) addition on an armchair edge [65,66] to form the fluorene-type configuration (Fig. 5(c)). Furthermore, the formation of the acenaphthene-type configuration (Fig. 5(b)) could also result from hydrogen addition to the acenaphthylene-type pentagonal rings [64]. To the best of our knowledge, our AFM/STM results represent the first observation of the existence of these two types of pentagonal rings. These findings may have some remarkable implications on the understanding of the soot formation mechanism, as will be discussed later.

Because of the frequent observation of acenaphthene-type five-membered rings among incipient soot molecules (Fig. 5(b)), we further validated their assignment by investigating the model compound 1,2-dihydro-3,5-dimethylbenz(J)aceanthrylene (DHDMBA, Sigma-Aldrich). The structure of DHDMBA is shown in Fig. 6(a) and contains an acenaphthene-type moiety, similar to the ones observed in soot molecules. Fig. 6(b)–(d) show AFM images of DHDMBA adsorbed on Cu(111), acquired with a CO-functionalized tip and at three different tip heights, together with the corresponding Laplace-filtered images. Because of the sp^3 hybridization, one of the two hydrogens for each C1 and C2 carbon atom is positioned above the plane of the molecular carbon backbone. As can be seen from the image at the largest tip-sample distance (Fig. 6(b), $z = 2.20$ Å), this results in an onset of repulsive forces already at larger tip-sample distances compared to the carbon backbone, and thus the -CH_2 moieties appear particularly bright in the AFM images (in fact, they appear almost as bright as the methyl groups at the C3 and C5 positions). The out-of-plane hydrogens also govern the contrast between the C1 and C2 carbons, causing the C1-C2 bond to appear elongated with respect to its actual length. This is due to the CO molecule tilting at the tip apex [23,27,67] and becomes more pronounced as the tip-sample distance is reduced (Fig. 6(c), $z = 2.45$ Å). At the smallest tip-sample distance probed here (Fig. 6(d), $z = 2.70$ Å), this effect also leads to the acenaphthene-type moiety appearing almost square-shaped. This characteristic evolution of the AFM contrast as a function of tip height is in very good agreement with the contrast observed on many of the soot molecules and allows us to assign this moiety with high certainty.

We can convert DHDMBA into its fully aromatic counterpart, 3,5-dimethylbenz(J)aceanthrylene (DMBA) by using atomic manipulation to selectively dissociate one hydrogen from each of the two -CH_2 moieties, as schematically depicted in Fig. 6(e). In Fig. 6(f), an AFM image of an intact DHMBA molecule is shown. Applying two consecutive voltage pulses of $V = 3.8$ V with the tip located above the molecule, we are able to successively remove one hydrogen from each CH_2 moiety and observe how the contrast in the AFM images changes (Fig. 6(f)–(h)). After the second pulse, we recover the usual contrast of an aromatic penta-ring, with brightness similar to those of the adjacent hexa-rings and apparent C1-C2 bond length closer to their actual values than in the doubly methylated molecule (Fig. 6(i)).

The presence of methylene C–H bonds results in a higher value of the H/C ratio of the soot molecules as compared to the purely benzenoid *peri*-condensed aromatics, commonly considered as precursors to soot. This is evidenced in Fig. 7, where the H/C ratio as function of the number of carbon atoms of the molecules (nC) is plotted considering only the aromatic network and neglecting the contribution of the aliphatic moieties. The dashed line corresponds to the lower limit of H/C for aromatic structures, which is met for purely *peri*-condensed PAHs. As reported by Solum et al. [68], this trend is a power law, i.e., $H/C = 1/(nC/6)^{\alpha}$ with $\alpha = 0.5$. For a given nC, any other aromatic structure, e.g., aromatic molecules with methylene C–H bonds, *cata*-condensed and/or cross-linked PAH, lies above the limit of *peri*-condensed PAH. Except for a few molecules such as **IS21** and **IS47**, whose main common characteristic is the pentagonal rings in acenaphthylene-type structure on *peri*-condensed cores (coronene for **IS21**, pyrene for **IS47**), all identified molecules exhibited equal or larger H/C ratios. This finding is corroborated by the fit to the experimental values obtained for the incipient soot molecules (black dots in Fig. 7) using the above-mentioned power law, yielding $\alpha = 0.43$. The imaged molecules exhibiting the highest H/C typically feature saturated peripheral penta-rings (sp^3 carbons), i.e., the molecules shown in Fig. 5(b) and (c). Further structural motifs containing methylene groups are observed, for example, in **IS6** and **IS56**, where saturated penta-rings are located on free edges of the molecule (Fig. 5(d)) as well as in **IS29, IS41, IS42, IS51** and **IS56**, which also feature methylene groups on peripheral benzenoid rings (Fig. 5).

The presence of such a large amount of methylene groups in soot molecules, mostly related to pentagonal rings, may explain some recent observations about the inception of soot [13]. Removal of a hydrogen atom from a methylene group (sp^3 hybridized carbon) induces a change of hybridization, resulting in the formation of a resonantly stabilized π-radical. In this case, the methylene carbon becomes sp^2 hybridized and, consequently, the unpaired electron is delocalized throughout the polyaromatic structure [69]. The formation of stable radicals via hydrogen abstraction from peripheral methylene groups was recently suggested to explain the large intensity of the corresponding m/z signal compared to the signal of a radical generated by removal of a hydrogen from a fully unsaturated PAH involved in the soot formation process [66]. On the other side, methylene groups in pentagonal rings may also

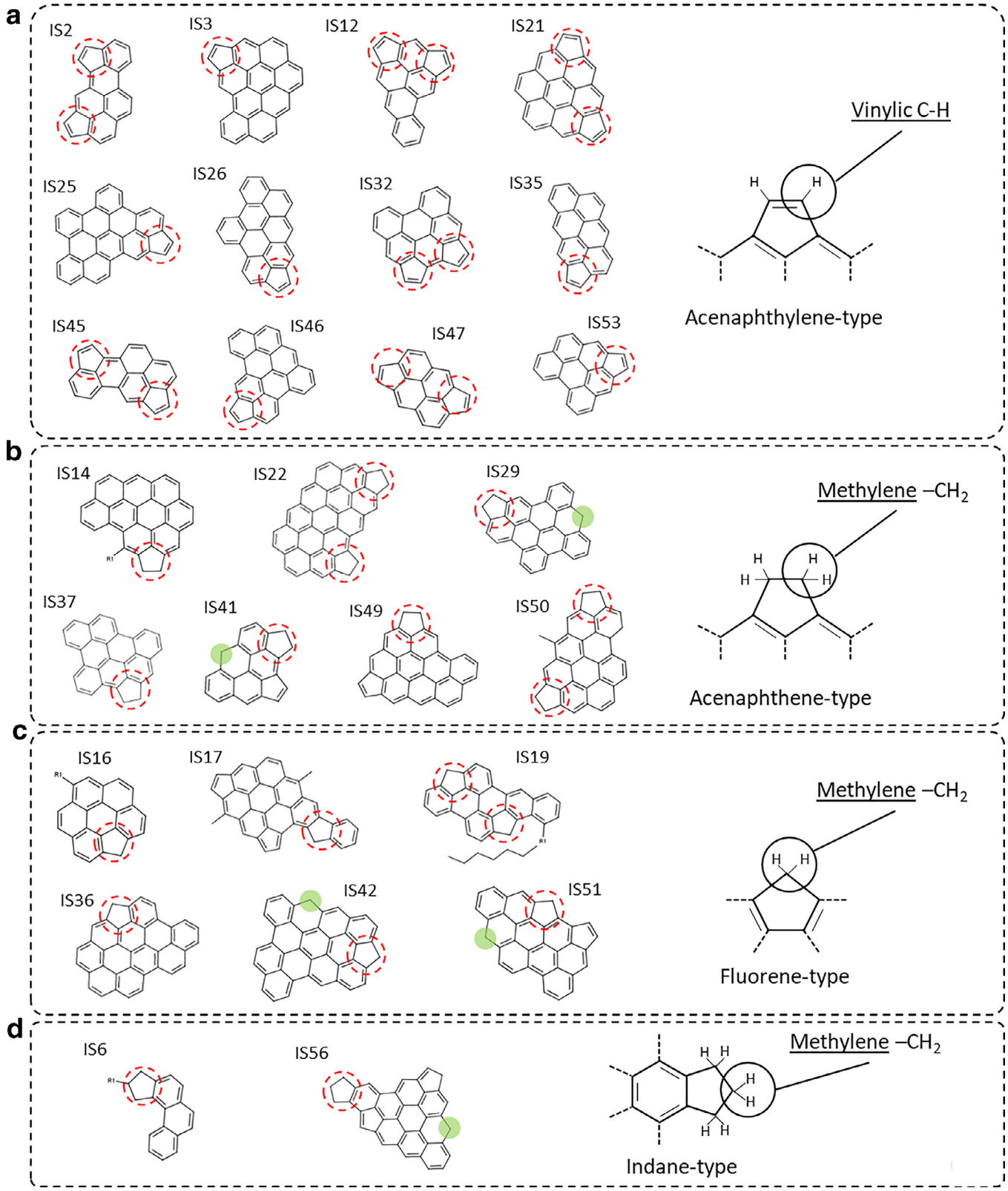

Fig. 5. Chemical structures of molecules with peripheral penta-ring assigned on the basis of AFM measurements shown in Fig. 2: (a) Molecules incorporating acenaphthylene-type moieties; (b) molecules incorporating acenaphthene-type moieties; (c) molecules incorporating fluorene-type moieties; (d) molecules with indane-type moieties. Dashed red circles are used as marker of the penta-ring position in the molecules; green dots indicate the position of methylene groups on peripheral benzenoid rings. (For interpretation of the references to color in this figure legend, the reader is referred to the web version of this article.)

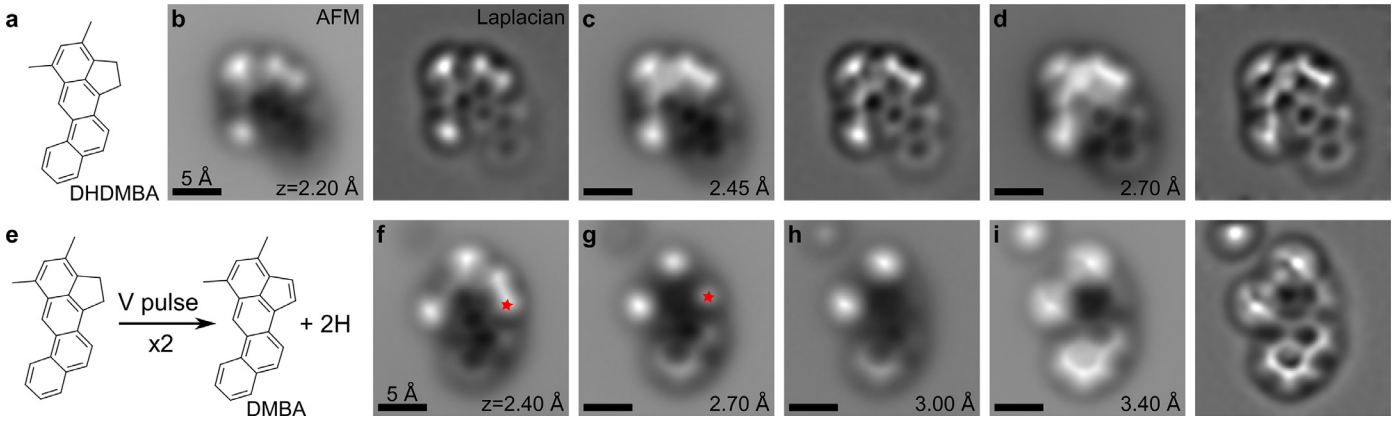

Fig. 6. (a) Chemical structure of acenaphthene-type model compound DHDMBA. (b)–(d) AFM images of DHDMBA at different tip-sample distances and corresponding Laplacian-filtered images. (e) Schematic of the conversion of DHDMBA to DMBA by tip-induced atomic manipulation. (f) AFM image of initially intact DHDMBA. The red star indicates the tip position for the application of the first voltage pulse to remove one hydrogen from the first -CH_2 moiety. (g) AFM image of the molecule after applying the first voltage pulse, with one H removed. (h) Image of the molecule after applying a second voltage pulse to also remove one H from the second -CH_2 moiety, yielding DMBA. (f) AMF image of DMBA at smaller tip-sample distance and corresponding Laplace-filtered image. z values correspond to the decrease in tip height with respect to the STM set point of $V = 0.2$ V, $I = 0.5$ pA. (For interpretation of the references to color in this figure legend, the reader is referred to the web version of this article.)

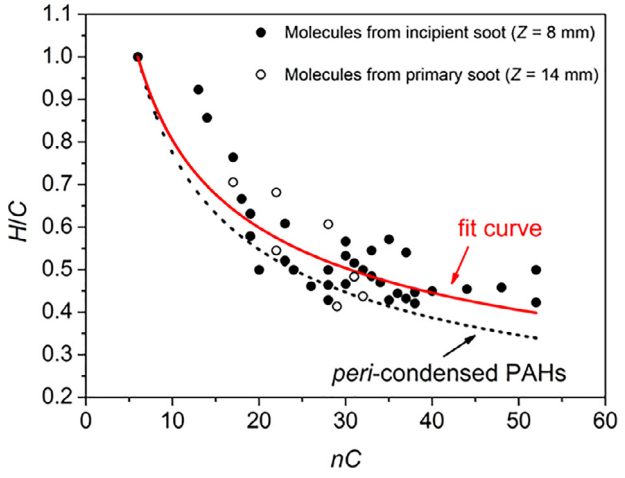

Fig. 7. H/C ratio as function of the number of aromatic carbon atoms (nC), obtained from the proposed chemical structures, excluding aliphatic side chains. The dashed line corresponds to the calculated trend for *peri*-condensed PAHs, i.e., $H/C = 1/(nC/6)^{0.5}$ [68]; the red line represents the best fit to the data obtained for the incipient soot molecules, using the relation $H/C = 1/(nC/6)^{\alpha}$ with $\alpha = 0.43$. (For interpretation of the references to color in this figure legend, the reader is referred to the web version of this article.)

be generated by hydrogen addition to a π-radical in a termination reaction of the radical-chain propagation mechanisms proposed by Johansson et al. [13]. In this context, the AFM molecules in Fig. 5 corroborate the mass spectrometric data of Johansson et al. [13], providing experimental evidences that resonantly stabilized π-radicals, activated by peripheral pentagonal rings, can play a fundamental role in the soot formation process.

Our AFM analysis also indicates the presence of such radicals among soot molecules, as apparent from the proposed chemical structures in Fig. 8(a). The π-radical **IS1**, for example, could have been formed by removal of a hydrogen atom from the C-atom highlighted in red, as proposed in Fig. 8(b), forming a delocalized unpaired electron (π-radical). For **IS10, IS58** and **PS3,** the assigned PAH core would indicate the presence of a π-radical. However, without knowledge of the exact substitutional group R1, this attribution remains uncertain.

Our results on delocalized π-radical formation allow a new interpretation of particle inception and can probably explain the dif-

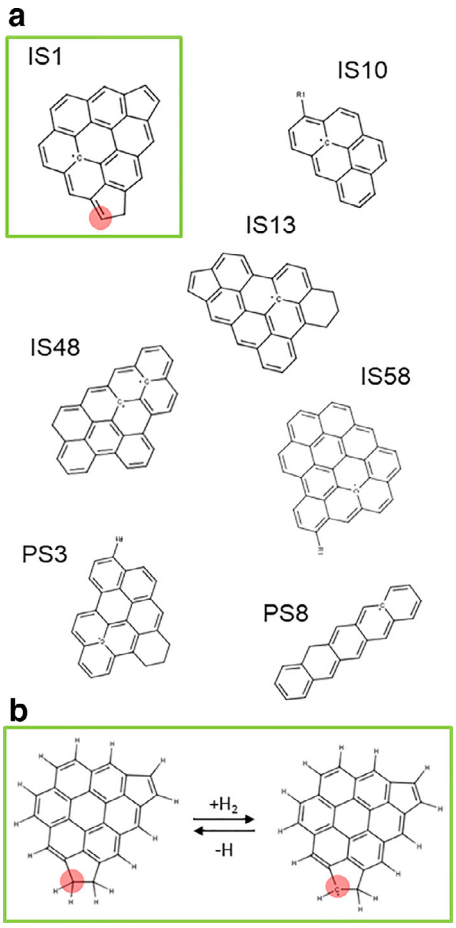

Fig. 8. (a) Proposed structure of imaged molecules with radical character. Note that multiple resonant structures are possible for all radicals depicted here. (b) Possible mechanism for the formation of a π-radical (forward reaction, one hydrogen is removed from the π-system resulting in a π-radical $+H_2$) and a methylene group (backward reaction, one hydrogen is added to the π-radical) in **IS1**. The carbon atom where a radical could have been formed is highlighted in red. (For interpretation of the references to color in this figure legend, the reader is referred to the web version of this article.)

ferent tendency to evaporate molecules from incipient ($Z = 8$ mm) and primary soot ($Z = 14$ mm). Incipient soot is composed of a large complexity of PAHs with different molecular sizes and shapes. These molecules are probably mostly held together by weak van der Waals forces and are in a condensed rather than a solid phase, so that they easily sublime without decomposing during sample preparation for AFM/STM imaging. As shown, such particles contain a high fraction of pentagonal rings, mostly located on the periphery of the aromatic molecules.

Soot particle growth is driven by H_2 release during molecular organization (the release of the gas-phase species accompanies the formation of highly ordered structures and causes an entropy increase, ultimately driving particle formation [8,11,60,70]). Hydrogen abstraction from purely benzenoid PAHs results in the formation of highly reactive aryl radicals. These radicals may promote either the formation of larger PAHs through acetylene addition and ring closure [8] or the formation of cross-linked structures when reacting with another aromatic [71]. It is commonly observed that the average size of the aromatic units (L_a) in flame-formed soot particles is on the order of 1 nm [14,50–52] and remains rather constant during the early stages of soot formation [14]. In our case, $L_a = 1.10$ nm for the incipient soot sample and 1.16 nm for the primary soot sample, as estimated by Raman spectroscopy (see supplementary materials S3). Thus, excluding a significant increase of the aromatic domains during soot particle growth, the formation of chemical bonds between the different aromatic units, i.e., formation of archipelago-type/cross-linked structures, is likely to play a fundamental role during the growth process of the soot particles from the nucleation region ($Z = 8$ mm) to the growth zone ($Z = 14$ mm). An evidence of cross-linking in incipient soot was clearly observed and discussed in our earlier work, where the AFM images as well as molecular orbital densities measured by STM and the corresponding DFT simulations were reported for the compound **IS43** in Fig. 2 (see Fig. 3 in Ref. [22]). The junction between the two aromatic subunits is a C–C bond formed between two pentagonal rings with hydrogen loss. In addition, **IS30** ($C_{52}H_{22}$ in Fig. 2 with respective structure in Fig. 4(b)), which is one of the largest molecules we found in the incipient soot, might have formed by the fusion of two pentagonal rings and H_2 loss. These molecules might indicate that chemical cross-linking between aromatics is promoted by the presence of peripheral penta-rings in the aromatic structures, thus representing a possible growth process for PAHs.

On the other hand, as discussed above, our observation of a large number of methylene groups results in the possibility of having many resonantly stabilized π-radicals within the pool of soot molecular constituents. Such polyaromatic radicals may be responsible for alternative mechanisms of soot formation and growth similar to the mechanism recently proposed by Johansson et al. [13]. Moreover, the presence of π-radicals may increase the binding forces among aromatics, as postulated for the clustering of phenalenyl-like radicals, which may form both σ and multicenter delocalized covalent-like bonds [72], thus enhancing the clustering/aggregation propensity of PAHs at the early stages of the soot formation process. Formation of such strong bonds could also be involved in the formation of grown primary soot particles and further explain why it was challenging to sublime the molecules from the sample of primary soot particles ($Z = 14$ mm). Finally, as already noticed by Wang and coauthors [12,55] and as recently pointed out by Johansson et al. [13], π-radicals may also explain the large amount of aliphatic moieties observed in the molecules of grown soot particles.

5. Conclusions

Incipient and early grown flame-formed soot particles, extracted from a slightly sooting ethylene/air premixed flame at two different flame positions, have been investigated at the single-molecule level by high-resolution atomic force microscopy.

A large complexity of molecular constituents of soot was found in both stages of soot formation. However, not all the features were present in both samples. Some common characteristics were the molecular masses, ranging from 200 to 700 Da with most molecular masses around 300 to 400 Da, as well as the distinct radical character of some molecules.

In incipient soot, we frequently observed molecules containing fused six-ring units organized in almost entirely *peri*-condensed structures and several molecules exhibiting aliphatic side-groups – mostly methyl (-CH_3) groups. In addition, many of the imaged molecules contained penta-rings on their periphery, while a smaller fraction showed penta-rings (partially) embedded into the aromatic structure. A large fraction of the peripheral penta-rings, as well as some hexa-rings, contained sp^3 hybridized carbons forming C–H bonds in methylene-type groups, which we confirmed by comparison with a model compound. This may have some implications on the understanding of molecule clustering and particle inception. Removal of a hydrogen atom from a methylene group (sp^3 hybridized carbon) induces a change of hybridization, resulting in the formation of a resonantly stabilized π-radical; the methylene carbon becomes sp^2 hybridized and the consequently unpaired electron is delocalized throughout the polyaromatic structure. On the other hand, methylene groups in pentagonal rings may also be generated by hydrogen addition to a π-radical, thus terminating the radical-chain propagation mechanisms pointed up by Johansson et al. [13]. Indeed, AFM analysis corroborated the presence of such radicals among the detected soot molecules. Moreover, AFM/STM gave the first direct evidence of the formation of archipelago-type/cross-linked structures, which are believed to play a role during the aging process of the soot particles.

In primary soot molecules, only a small number of PAHs could be found on the substrate surface after sublimation. Together with our findings on resonantly stabilized π-radicals, this indicates that an increase in binding forces between aromatics due to the presence of radicals might foster the clustering/aggregation process of PAHs at the early stages of soot formation. The formation of σ and/or multicenter delocalized covalent-like bonds between the aromatic constituents can lead to fragmentation rather than sublimation during the sample preparation. Moreover, the presence of π-radicals might explain the high aliphatic content found in the soot molecules and possibly the formation of oxygen-bonded molecules that have been found in primary soot.

Acknowledgments

We thank R. Allenspach for comments and discussions. This work was financially supported by the ERC Consolidator Grant AMSEL (682144) and by “Accordo di Programma CNR-MSE Ricerca di Sistema Elettrico” – Project “MIcro co/tri generazione di Bioenergia Efficiente e Stabile (Mi-Best)”.

Supplementary material

Supplementary material associated with this article can be found, in the online version, at doi:10.1016/j.combustflame.2019.03.042.

References

[1] International Energy Agency, World Energy Outlook 2018, 13 Nov 2018, ISBN: 9789264306776, doi:10.1787/weo-2018-en.
[2] C.I. Davidson, R.F. Phalen, P.A. Solomon, Airborne particulate matter and human health: a review, Aerosol. Sci. Technol. 39 (8) (2005) 737–749.
[3] I.M. Kennedy, The health effects of combustion-generated aerosols, Proc. Combust. Inst. 31 (2007) 2757–2770.
[4] P. Pedata, T. Stoeger, R. Zimmermann, A. Peters, G. Oberdörster, A. D'Anna, Are we forgetting the smallest, sub 10 nm combustion generated particles? Part. Fibre Toxicol. 12 (2015) 34.
[5] G. Oberdörster, Z. Sharp, V. Atudorei, A. Elder, R. Gelein, W. Kreyling, C. Cox, Translocation of inhaled ultrafine particles to the brain, *Inhal. Toxicol.* 16 (6-7) (2004) 437–445.
[6] T.C. Bond, S.J. Doherty, D.W. Fahey, P.M. Forster, T. Berntsen, B.J. DeAngelo, et al., Bounding the role of black carbon in the climate system: a scientific assessment, J. Geophys. Res.: Atmos. 118 (2013) 5380–5552.
[7] J. Hansen, L. Nazarenko, Soot climate forcing via snow and ice albedos, Proc. Natl. Acad. Sci. 101 (2004) 423–428.
[8] M. Frenklach, D.W. Clary, W.C. Gardiner Jr., S.E. Stein, Detailed kinetic modeling of soot formation in shock-tube pyrolysis of acetylene, Symp. (Int.) Combust. 20 (1985) 887–901.
[9] M. Frenklach, H. Wang, Detailed modeling of soot particle nucleation and growth, Symp. (Int.) Combust. 23 (1991) 1559–1566.
[10] M. Frenklach, Reaction mechanism of soot formation in flames, Phys. Chem. Chem. Phys. 4 (2002) 2028–2037.
[11] A. D'Anna, Combustion-formed nanoparticles, Proc. Combust. Inst. 32 (2009) 593–613.
[12] H. Wang, Formation of nascent soot and other condensed-phase materials in flames, Proc. Combust. Inst. 33 (2011) 41–67.
[13] K.O. Johansson, M.P. Head-Gordon, P.E. Schrader, K.R. Wilson, H.A. Michelsen, Resonance-stabilized hydrocarbon-radical chain reactions may explain soot inception and growth, Science 361 (2018) 997–1000.
[14] M. Commodo, G. De Falco, A. Bruno, C. Borriello, P. Minutolo, A. D'Anna, Physicochemical evolution of nascent soot particles in a laminar premixed flame: from nucleation to early growth, Combust. Flame 162 (2015) 3854–3863.
[15] F. Carbone, M. Attoui, A. Gomez, Challenges of measuring nascent soot in flames as evidenced by high resolution differential mobility analysis, Aerosol Sci. Technol. 50 (2016) 740–757.
[16] Q. Tang, R. Cai, X. You, J. Jiang, Nascent soot particle size distributions down to 1 nm from a laminar premixed burner-stabilized stagnation ethylene flame, Proc. Combust. Inst. 36 (2017) 993–1000.
[17] B. Zhao, Z. Yang, J. Wang, M.V. Johnston, H. Wang, Analysis of soot nanoparticles in a laminar premixed ethylene flame by scanning mobility particle sizer, Aerosol Sci. Technol. 37 (2003) 611–620.
[18] L.A. Sgro, A. D'Anna, P. Minutolo, Charge fraction distribution of nucleation mode particles: new insight on the particle formation mechanism, Combust. Flame 158 (2011) 1418–1425.
[19] M. Alfè, B. Apicella, R. Barbella, J.-N Rouzaud, A. Tregrossi, A. Ciajolo, Structure-property relationship in nanostructures of young and mature soot in premixed flames, Proc. Combust. Inst. 32 (2009) 697–704.
[20] F. Migliorini, K.A. Thomson, G.J. Smallwood, Investigation of optical properties of aging soot, Appl. Phys. B 104 (2011) 273–283.
[21] M. Commodo, A. D'Anna, G. De Falco, R. Larciprete, P. Minutolo, Illuminating the earliest stages of the soot formation by photoemission and Raman spectroscopy, Combust. Flame 181 (2017) 1339–1351.
[22] F. Schulz, M. Commodo, K. Kaiser, G. De Falco, P. Minutolo, G. Meyer, A. D'Anna, L. Gross, Insights into incipient soot formation by atomic force microscopy, Proc. Combust. Inst. 37 (2019) 885–892.
[23] L. Gross, F. Mohn, N. Moll, P. Liljeroth, G. Meyer, The chemical structure of a molecule resolved by atomic force microscopy, Science 325 (2009) 1110–1114.
[24] P. Hapala, G. Kichin, C. Wagner, F.S. Tauz, R. Temirov, P. Jelínek, Mechanism of high-resolution STM/AFM imaging with functionalized tips, Phys. Rev. B 90 (8) (2014) 085421.
[25] K.Ø. Hanssen, B. Schuler, A.J. Williams, T.B. Demissie, E. Hansen, J.H. Andersen, J. Svenson, K. Blinov, M. Repisky, F. Mohn, G. Meyer, J.-S. Svendsen, K. Ruud, M. Elyashberg, L. Gross, M. Jaspars, J. Isaksson, A combined atomic force microscopy and computational approach for the structural elucidation of Breitfussin A and B: highly modified halogenated dipeptides from Thuiaria breitfussi, Angew. Chem. Int. Ed. 51 (2012) 12238–12241.
[26] B. Schuler, G. Meyer, D. Peña, O.C. Mullins, L. Gross, Unraveling the molecular structures of asphaltenes by atomic force microscopy, J. Am. Chem. Soc. 137 (2015) 9870–9876.
[27] B. Schuler, S. Fatayer, G. Meyer, E. Rogel, M. Moir, Y. Zhang, M.R. Harper, A.E. Pomerantz, K.D. Bake, M. Witt, D. Peña, J.D. Kushnerick, O.C. Mullins, C. Ovalles, F.G.A. van den Berg, L. Gross, Heavy oil based mixtures of different origins and treatments studied by atomic force microscopy, Energy Fuels 31 (2017) 6856–6861.
[28] L. Gross, F. Mohn, N. Moll, B. Schuler, A. Criado, E. Guitián, D. Peña, A. Gourdon, G. Meyer, Bond-order discrimination by atomic force microscopy, Science 337 (2012) 1326–1329.
[29] D.G. de Oteyza, P. Gorman, Y.-C. Chen, S. Wickenburg, A. Riss, D.J. Mowbray, G. Etkin, Z. Pedramrazi, H.Z. Tsai, A. Rubio, M.F. Crommie, F.R. Fischer, Direct imaging of covalent bond structure in single-molecule chemical reactions, Science 340 (2013) 1434–1437.
[30] F. Schulz, P.H. Jacobse, F.F. Canova, J. van der Lit, D.Z. Gao, A. van den Hoogenband, P. Han, R.J.M. Klein Gebbink, M.-E. Moret, P.M. Joensuu, I. Swart, P. Liljeroth, Precursor geometry determines the growth mechanism in graphene nanoribbons, J. Phys. Chem. C 121 (2017) 2896–2904.
[31] J. Repp, G. Meyer, S.M. Stojković, A. Gourdon, C. Joachim, Molecules on insulating films: scanning-tunneling microscopy imaging of individual molecular orbitals, Phys. Rev. Lett. 94 (2005) 026803.
[32] L. Gross, N. Moll, F. Mohn, A. Curioni, G. Meyer, F. Hanke, M. Persson, High--resolution molecular orbital imaging using a p-wave STM tip, Phys. Rev. Lett. 107 (2011) 086101.
[33] F. Schulz, M. Ijäs, R. Drost, S.K. Hämäläinen, A. Harju, A.P. Seitsonen, P. Liljeroth, Many-body transitions in a single molecule visualized by scanning tunnelling microscopy, Nat. Phys. 11 (2015) 229–234.
[34] F.J. Giessibl, High-speed force sensor for force microscopy and profilometry utilizing a quartz tuning fork, App. Phys. Lett. 73 (1998) 3956.
[35] T.R. Albrecht, P. Grütter, D. Horne, D. Rugar, Frequency modulation detection using high-Q cantilevers for enhanced force microscope sensitivity, J. Appl. Phys. 69 (1991) 668–673.
[36] L. Bartels, G. Meyer, K.-H. Rieder, Controlled vertical manipulation of single CO molecules with the scanning tunneling microscope: a route to chemical contrast, Appl. Phys. Lett. 71 (1997) 213–215.
[37] R.J. Beuhler, E. Flanigan, L.J. Greene, L. Friedman, Proton transfer mass spectrometry of peptides. A rapid heating technique for underivatized peptides containing arginine, J. Am. Chem. Soc. 96 (12) (1974) 3990–3999.
[38] T. Zambelli, P. Jiang, J. Lagoute, S.E. Grillo, S. Gauthier, A. Gourdon, C. Joachim, Deformation of a 3.7-nm long molecular wire at a metallic step edge, Phys. Rev. B 66 (7) (2002) 754101–754107.
[39] B. Schuler, Y. Zhang, S. Collazos, S. Fatayer, G. Meyer, D. Pérez, E. Guitián, M.R. Harper, J.D. Kushnerick, D. Peña, L. Gross, Characterizing aliphatic moieties in hydrocarbons with atomic force microscopy, Chem. Sci. 8 (3) (2017) 2315–2320.
[40] L. Grill, Large molecules on surfaces: deposition and intramolecular STM manipulation by directional forces, J. Phys. Condens. Matter 22 (8) (2010) 084023.
[41] R.A. Dobbins, R.A. Fletcher, W. Lu, Laser microprobe analysis of soot precursor particles and carbonaceous soot, Combust. Flame 100 (1995) 301–309.
[42] R.A. Dobbins, R.A. Fletcher, H.-C. Chang, The evolution of soot precursor particles in a diffusion flame, Combust. Flame 115 (1998) 285–298.
[43] S. Stein, A. Fahr, High-temperature stabilities of hydrocarbons, J. Phys. Chem. 89 (1985) 3714–3725.
[44] S.A. Skeen, H.A. Michelsen, K.R. Wilson, D.M. Popolan, A. Violi, N. Hansen, Near-threshold photoionization mass spectra of combustion-generated high–molecular-weight soot precursors, J. Aerosol Sci. 58 (2013) 86–102.
[45] K.O. Johansson, J.Y.W. Lai, S.A. Skeen, D.M. Popolan-Vaida, K.R. Wilson, N. Hansen, A. Violi, H.A. Michelsen, Soot precursor formation and limitations of the stabilomer grid, Proc. Combust. Inst. 35 (2015) 1819–1826.
[46] K.O. Johansson, J. Zádor, P. Elvati, M.F. Campbell, P.E. Schrader, N.K. Richards-Henderson, K.R. Wilson, A. Violi, H.A. Michelsen, Critical assessment of photoionization efficiency measurements for characterization of soot-precursor species, J. Phys. Chem. A 121 (2017) 4475–4485.
[47] K.O. Johansson, T. Dillstrom, P. Elvati, M.F. Campbell, P.E. Schrader, D.M. Popolan-Vaida, N.K. Richards-Henderson, K.R. Wilson, A. Violi, H.A. Michelsen, Radical–radical reactions, pyrene nucleation, and incipient soot formation in combustion, Proc. Combust. Inst. 36 (2017) 799–806.
[48] Y. Bouvier, C. Mihesan, M. Ziskind, E. Therssen, C. Focsa, J.F. Pauwels, P. Desgroux, Molecular species adsorbed on soot particles issued from low sooting methane and acetylene laminar flames: a laser-based experiment, Proc. Combust. Inst. 31 (2007) 841–849.
[49] B. Öktem, M.P. Tolocka, B. Zhao, H. Wang, M.V. Johnston, Chemical species associated with the early stage of soot growth in a laminar premixed ethylene–oxygen–argon flame, Combust. Flame 142 (2005) 364–373.
[50] M.L. Botero, E.M. Adkins, S. González-Calera, H. Miller, M. Kraft, PAH structure analysis of soot in a non-premixed flame using high-resolution transmission electron microscopy and optical band gap analysis, Combust. Flame 164 (2016) 250–258.
[51] E.M. Adkins, J.A. Giaccai, J.H. Miller, Computed electronic structure of polynuclear aromatic hydrocarbon agglomerates, Proc. Combust. Inst. 36 (2017) 957–964.
[52] B. Apicella, P. Pré, M. Alfè, A. Ciajolo, V. Gargiulo, C. Russo, A. Tregrossi, D. Deldique, J.N. Rouzaud, Soot nanostructure evolution in premixed flames by high resolution electron transmission microscopy (HRTEM), Proc. Combust. Inst. 35 (2015) 1895–1902.
[53] J.P. Cain, J. Camacho, D.J. Phares, H. Wang, A. Laskin, Evidence of aliphatics in nascent soot particles in premixed ethylene flames, Proc. Combust. Inst. 33 (2011) 533–540.
[54] C. Russo, F. Stanzione, A. Tregrossi, A. Ciajolo, Infrared spectroscopy of some carbon-based materials relevant in combustion: qualitative and quantitative analysis of hydrogen, Carbon 74 (2014) 127–138.
[55] J.P. Cain, PL. Gassman, H. Wang, A. Laskin, Micro-FTIR study of soot chemical composition—evidence of aliphatic hydrocarbons on nascent soot surfaces, Phys. Chem. Chem. Phys. 12 (2010) 5206–5218.
[56] A. Santamaría, F. Mondragón, A. Molina, N.D. Marsh, E.G. Eddings, A.F. Sarofim, FT-IR and 1H NMR characterization of the products of an ethylene inverse diffusion flame, Combust. Flame 146 (2006) 52–62.
[57] P. Minutolo, G. Rusciano, L.A. Sgro, G. Pesce, A. Sasso, A. D'Anna, Surface en-

hanced Raman spectroscopy (SERS) of particles produced in premixed flame across soot threshold, Proc. Combust. Inst. 33 (2011) 649–657.
[58] P. Elvati, A. Violi, Thermodynamics of poly-aromatic hydrocarbon clustering and the effects of substituted aliphatic chains, Proc. Combust. Inst. 34 (2013) 1837–1843.
[59] H.W. Kroto, K. McKay, The formation of quasi-icosahedral spiral shell carbon particles, Nature 331 (1988) 328–331.
[60] R. Whitesides, M. Frenklach, Detailed kinetic Monte Carlo simulations of graphene-edge growth, J. Phys. Chem. A 114 (2010) 689–703.
[61] E.M. Adkins, J.H. Miller, Towards a taxonomy of topology for polynuclear aromatic hydrocarbons: linking electronic and molecular structure, Phys. Chem. Chem. Phys. 19 (2017) 28458–28469.
[62] J.W. Martin, K. Bowal, A. Meno, R.I. Slavchov, J. Akroyd, S. Mosbach, M. Kraft, Polar curved polycyclic aromatic hydrocarbons in soot formation, Proc. Comb. Inst. 37 (2019) 1117–1123.
[63] M. Frenklach, C.A. Schuetz, J. Ping, Migration mechanism of aromatic-edge growth, Proc. Comb. Inst. 37 (2005) 1389–1396.
[64] B. Shukla, M. Koshi, A novel route for PAH growth in HACA based mechanisms, Combust. Flame 159 (2012) 3589–3596.
[65] B. Shukla, A. Miyoshi, M. Koshi, Role of methyl radicals in the growth of PAHs, J. Am. Soc. Mass. Spectrom. 21 (2010) 534–544.
[66] M. Schenk, N. Hansen, H. Vieker, A. Beyer, A. Gölzhäuser, K. Kohse-Höinghaus, PAH formation and soot morphology in flames of C4 fuels, Proc. Combust. Inst. 35 (2015) 1761–1769.
[67] S.K. Hämäläinen, N.J. Van Der Heijden, J. Van Der Lit, S. Den Hartog, P. Liljeroth, I. Swart, Intermolecular contrast in atomic force microscopy images without intermolecular bonds, Phys. Rev. Lett. 113 (18) (2014) 1–5.
[68] M.S. Solum, R.J. Pugmire, D.M. Grant, Carbon-13 solid-state NMR of Argonne-premium coals, Energy Fuels 3 (1989) 187–193.
[69] J.B. Howard, Carbon addition and oxidation reactions in heterogeneous combustion and soot formation, Symp. (Int.) Combust. 23 (1991) 1107–1127.
[70] M. Frenklach, R.I. Singh, A.M. Mebel, On the low-temperature limit of HACA, Proc. Combust. Inst. 37 (2019) 969–976.
[71] A. D'Anna, A. Violi, A. D'Alessio, A. Sarofim, A reaction pathway for nanoparticle formation in rich premixed flames, Combust. Flame 127 (2001) 1995–2003.
[72] Z. Mou, K. Uchida, T. Kubo, M. Kertesz, Evidence of σ- and π-dimerization in a series of phenalenyls, J. Am. Chem. Soc. 136 (2014) 18009–18022.